water

MDPI

Article

Radioactivity of Soil, Rock and Water in a Shale Gas Exploitation Area, SW China

Tianming Huang [1,2,*], Yinlei Hao [1,2], Zhonghe Pang [1,2], Zhenbin Li [1,2] and Shuo Yang [1,2]

[1] Key Laboratory of Shale Gas and Geoengineering, Institute of Geology and Geophysics, Chinese Academy of Sciences, Beijing 100029, China; ylhao@mail.iggcas.ac.cn (Y.H.); z.pang@mail.iggcas.ac.cn (Z.P.); lizhenbin16@mails.ucas.ac.cn (Z.L.); yangshuo@mail.iggcas.ac.cn (S.Y.)

[2] College of Earth Sciences, University of Chinese Academy of Sciences, Beijing 100049, China

* Correspondence: tmhuang@mail.iggcas.ac.cn; Tel.: +86-10-8299-8276

Academic Editor: Maurizio Barbieri

Received: 25 January 2017; Accepted: 19 April 2017; Published: 26 April 2017

Abstract: Studies have been carried out to investigate the baseline radioactivity level (gross alpha, gross beta and ^{226}Ra) of soil, rocks and groundwater in the Fuling block, Chongqing, the largest shale gas exploitation area of China. The results show that there is a general activity concentration trend of gross alpha, gross beta and ^{226}Ra: shale > soil > limestone due to the high content of uranium, thorium and potassium in shale and low content in limestone. The average activities of shallow groundwater from a limestone aquifer are 0.14, 0.13 and <0.008 Bq/L for gross alpha, gross beta and ^{226}Ra, respectively. The radioactivity concentrations of gross alpha, gross beta and ^{226}Ra (4.37, 1.40 and 0.395 Bq/L, respectively) of the formation water were far lower than those of formation water in the Marcellus shale in the USA (with ranges of 86–678, 23–77 and 16–500 Bq/L, respectively). One polluted shallow groundwater source and its associated stream sediments had been polluted due to leakage of drilling fluid with relatively high radioactivity levels and high concentration of main ions. Overall, this study provides an important baseline radioactivity level to assess the impact of shale gas exploitation on a shallow environment.

Keywords: radioactivity; shale gas; gross alpha; gross beta; ^{226}Ra

1. Introduction

With the rapid development of horizontal drilling and large-scale hydraulic fracturing, the production of shale gas has substantially expanded [1]. At the same time, concerns regarding potential environmental pollution from hydraulic fracturing have also arisen [2,3], especially the potential contamination of shallow aquifers by hydraulic fracturing fluids and/or formation water from deep formations through induced and natural fractures [4], leaking from casings and cement or wastewater discharge [1,5]. Of the complex contaminants in hydraulic fracturing fluids and/or formation water, naturally occurring radioactive materials (NORM) are notable concerns [6–8]. For example, Warner et al. [9] found that the radioactivity level of ^{226}Ra in stream sediments at the point of discharge at a waste treatment facility in central Pennsylvania was nearly 200 times greater than those of upstream and background sediments. While most attention has focused on radium [9–11], few reports regarding the general radioactivity levels are available [12]. As radioactive isotopes decay by emitting alpha and beta particles, alpha and beta activities can serve as rough indicators of the presence of radioactive elements [13]. In addition, some studies have indicated that the high radioactivity in the flowback and produced waters can reflect naturally occurring brines, which are associated with the targeted formations [4,11]. However, there is a lack of studies on the radioactivity levels of these different reservoirs as well as the relationship of radioactivity between waters and their reservoirs

related to shale gas exploitation. Therefore, the general radioactivity levels are assessed by the activity concentrations of gross alpha (gross-α), gross beta (gross-β) and ^{226}Ra in this study.

China has the second largest shale gas reserves, with approximately 1/13 of the world reserves [14]. Shale gas development entered industrial testing and the early stages of commercial development during 2011–2015 and will be industrialized at a large scale in the next five years, with the yield of shale gas expected to be 30 billion m^3/year in 2020 [15]. Assessing the risk of water and soil contamination, establishing a long-term monitoring system, and studying the transport mechanism of water and pollutants through a fracture are necessary during this period. The Fuling block is the largest shale gas exploitation area in China, with a shale gas yield of 5 billion m^3/year in 2016 (10 billion m^3/year is expected in 2020). As the first and largest commercial-scale shale gas production area in China, assessing the impact of shale gas exploitation on shallow environments (groundwater and soil) can provide an important case study.

Some studies have assessed the baseline level of the methane content, major ions and typical toxic elements of shallow groundwater in the Fuling shale gas area [16]. However, there is no study on the radioactivity levels of different reservoirs. In this study, the activity of gross-α, gross-β and ^{226}Ra in soil, rocks (limestone and shale) and waters (shallow karst groundwater, formation water and flowback fluid) will be assessed and compared with those of other similar areas. The data obtained in this study will provide important baseline values of the radioactivity in soils, rocks, and shallow groundwater, and are helpful to examine the possible contamination of shallow groundwater and sediments by leakage of flowback fluid or formation water in this shale gas exploitation area.

2. Study Area

The study area is located in eastern Chongqing, SW China. The Fuling block contains an anticline that is confined by faults on the basin boundary. The Lower Silurian Longmaxi (S_1l) shale is the product formation for shale gas exploitation in this block, which is buried successively under Lower Silurian Xiaheba shale (S_1x, depth of 200 m), Middle Silurian Hanjiadian mudstone and silt mudstone (S_2h depth of 500 m), Permian (P, depth of 720 m) and Triassic (T) carbonate rock (depth of 800 m) based on the borehole JY1 (the location can be found in Figure 1). The S_1l is one of the most important marine shale gas plays in southern China [17] and the Fuling bock is the largest shale gas exploitation area in China, with a shale gas yield of 5 billion m^3/year in 2016. The lithology of the shallow groundwater aquifer is all limestone and dolomite, which are from the Lower Triassic Jianglingjiang group (T_1j) at a depth of 300 m, Feixianguan group (T_1f, 500 m), Upper Permian (P_2) at a depth of 230 m and Lower Permian (P_1, 490 m). The shale gas exploitation field is mainly located in middle and low mountainous areas with a surface lithology of T_1j, where the discharge of a large spring and underground river ranges from 100 to 1000 L/s and the runoff modulus is more than 6 L/s·km^2 (Figure 1). Although the lithology of the shallow aquifer is simple, the groundwater and cave spring (outcrop of karst groundwater) distribute unevenly. The shallow groundwater aquifer mainly distributes in the upper 150 m of the limestone [18].

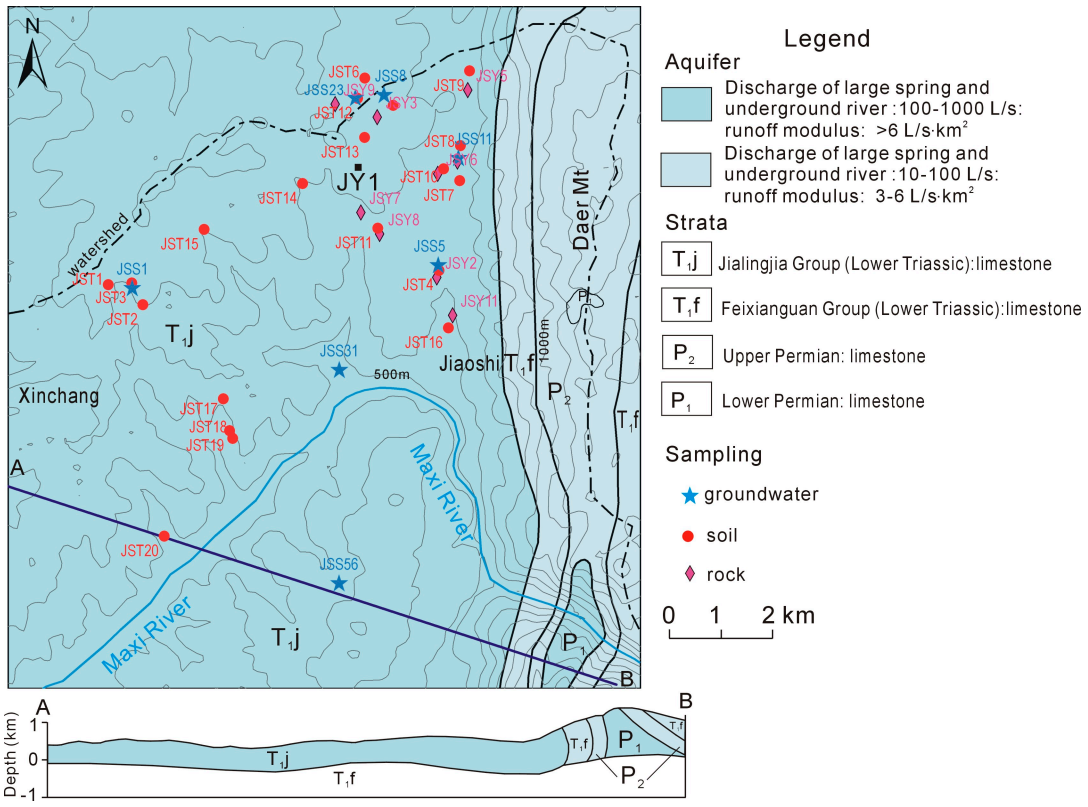

Figure 1. Study area and sampling locations.

3. Samples and Analyses

Groundwater samples mostly came from the karst caves in the study area. Other samples included a groundwater sample polluted by drilling fluid leakage (JSS23), one formation water of shale (JSS31) and one flowback fluid of hydraulic fracturing (JSS56). Soil (18 samples), surface fresh core (T_1j, 10 samples) and shale (S_1l, two samples) were sampled. In addition, two stream sediments (JST 12 and JST 13) following the karst cave sample of JSS23 were sampled to study the impact of the fluid leakage.

Water chemistry and trace element analyses were performed in the Beijing Research Institute of Uranium Geology (BRIUG). Anions (F, Cl, SO_4 and NO_3, detection limit of 0.05 mg/L) were measured with a DIONEX-500 Ion Chromatograph and HCO_3 and CO_3 were measured by a 785DMP titrator (accuracy is ±5 mg/L). Cations (K, Na, Ca, Mg) were analyzed by Inductively Coupled Plasma Optical Emission Spectroscopy (ICP-OES) with a detection limit of 0.05 mg/L. Trace elements (Ba, Sr, Li, U, and Th) were determined by Inductively Coupled Plasma Mass Spectrometry (ICP-MS). The standard of trace element was ICP-MS Complete Standard (IV-ICPMS-71A). The detect limit was 0.005 μg/L.

The mineral compositions for soil and rock samples were analyzed by X-Ray Diffraction (XRD). Major elements were analyzed with a Philips PW 2400 X-ray fluorescence spectrometer (Amsterdam, The Netherlands), yielding analytical uncertainties better than ±5% (2σ). Trace element was estimated by inductively-coupled plasma mass spectrometry (ICP-MS) with NexION 300D (PerkinElmer Inc., Shelton, CT, USA). The standards of trace element for solid sample were the National standards GBW07104 with andesite as matrix and GBW07312 with stream sediment as matrix. The detect limit was 0.005 μg/g.

The radium isotope (^{226}Ra) was determined mainly according to the national standard of Analytical Determination of ^{226}Ra in water (GB/T8538-2008). Ba and Pb carriers were added to the acidified sample (4 L) and Ra isotopes were coprecipitated on (Ba, Pb) SO_4 by adding dilute H_2SO_4. The precipitate was aged by standing overnight, centrifuged and discarded supernate. Then

the precipitate was dissolved in EDTA (ethylenediaminetetraacetic acid) and transferred to an Rn bubbler where ^{222}Rn was allowed to grow by standing for 14 days. After ingrowth, the gas was purged into a scintillation cell the sample was stored for 3 h to allow equilibrium to be reached between ^{222}Rn and its short-lived progeny [19]. Then the cell was placed in the PC 2100 Radium and Radon Analyzer [20] for α-particle counting in the BRIUG. The principle is that the internal surface of the scintillation cell is coated with silver-activated zinc sulfide, ZnS(Ag), the alpha-particles produced by the decay of ^{222}Rn and its short-lived decay products transfer their energy as they pass through the scintillation medium emit photons from the ZnS(Ag) coating that can be detected by a photomultiplier. The photomultiplier converts the photons into electrical pulses that are then counted. The pulse count is directly proportional to the activity concentration of radon and its decay products present in the scintillation cell. Then the ^{226}Ra activity concentration can be calculated taking into account the known steady state between ^{226}Ra and ^{222}Rn [20]. The detection limit [21] was 0.008 Bq/L. Calibration of the α scintillation cell and the counting instrument was performed with a standard source of ^{226}Ra (GBW04312) prepared in the same geometry as the samples to be measured. For ^{226}Ra measurements of soil and rock, 2.000 g sample with particle sizes less than 0.074 mm were melted at 650 °C for 10 min with addition of Na_2O_2 and NaOH and then acidified by HCl. The latter procedure was the same with water samples by means of the PC 2100 Radium and Radon Analyzer. The high content standardized radium material dissolved directly and sealed. Then the standard radium material was done with the samples and the procedure was performed in the same manner as the samples. The losses of mass are accounted by the standard material's recovery rate of entire experiment. ^{133}Ba was also measured to determine chemical yield [22,23].

For gross-α and gross-β in groundwater, samples were evaporated, dried at 450 °C for 30 min. The sample residues were cooled in the desiccator, and then weighed. Later, the sample residues were grinded to ensure that the particle size was homogeneous. About 0.3000 g of the sample residues was taken for measurement of the gross alpha and gross beta radioactivity, transferred into a 2-inch diameter stainless steel planchet, evenly spread, fixed with acetone and dried under an infrared lamp. Counted for alpha and beta activity by means of a MINI20 Low-background α&β instrument was manufactured by Eurysis Mesure, France. The detection limits of gross-α and gross-β are 0.022 and 0.003 Bq/L, respectively. Calibration was done using ^{241}Am (JZ-A21-140513A201) certified reference sources for alpha and KCl standard for beta. Counting time for samples and background was 60 min. The alpha and beta efficiencies were both $\geq$30%. The background readings of the detector for alpha and beta activity concentrations were $\leq$0.06 and <0.4 cpm, respectively. Soil and rock samples were homogeneously pulverized and directly measured by the same instrument. The results are provided in Tables 1–3.

Table 1. The activities of soil (including polluted stream sediments) and rock (including limestone and shale) as well as mineral and chemical composition (U and Th) (Q: quartz; Pl: plagioclase; Ca: calcite; D: dolomite; Py: pyrite; Cl: clay).

Type	Q	Pl	Ca	D	Py	Cl	Gross-α	Gross-β	^{226}Ra	U	Th	K	^{238}U *	^{40}K *	^{226}Ra/^{238}U *	X *
	%						Bq/kg			μg/g		%	Bq/kg			$A_{K-\beta}/A_{Gross-\beta}$
soil																
JST1	81.9	/	/	/	/	18.1	715	865	16	1.59	7.31	1.65	28	523	0.56	0.54
JST2	85.2	/	/	/	/	14.8	591	568	26	1.69	6.37	1.86	30	590	0.86	0.93
JST3	60.4	/	/	/	/	39.6	1340	1630	78	8.33	15.30	3.02	148	957	0.53	0.52
JST4	62.6	/	/	/	/	37.4	2650	1330	68	7.92	16.30	3.07	141	973	0.48	0.65
JST5	62.4	/	/	6.0	/	31.6	1420	1030	61	5.57	15.00	2.42	99	767	0.61	0.66
JST6	73.0	/	/	/	/	27.0	1510	796	41	4.31	12.40	2.21	77	701	0.53	0.79
JST7	43.3	/	/	/	/	56.7	1060	1380	67	9.55	17.30	2.10	170	666	0.39	0.43
JST8	70.9	/	/	/	/	29.1	1460	983	42	5.47	12.80	1.69	97	536	0.43	0.49
JST9	61.0	/	2.0	6.2	/	30.8	2360	2220	51	5.60	13.90	2.40	100	761	0.51	0.31
JST10	48.8	/	/	/	/	51.2	2120	1830	82	9.45	17.70	2.66	168	843	0.49	0.41
JST11	51.4	/	/	/	/	48.6	1160	1240	80	6.79	15.90	1.87	121	593	0.66	0.43
JST14							1810	1190	56							
JST15	61.2	/	/	11.9	/	26.9	2130	1310	70	5.06	14.20	1.92	90	609	0.78	0.41
JST16	63.4	/	/	/	/	36.6	1480	1210	81	8.10	15.10	2.35	144	745	0.56	0.55
JST17	63.9	/	14.3	/	/	21.8	2160	1420	56	4.88	13.70	2.93	87	929	0.64	0.58
JST18	33.9	/	30.4	19.8	/	15.9	1400	758	48	3.86	10.10	1.78	69	564	0.70	0.66
JST19							810	723	46							
JST20	58.4	/	4.6	/	/	37.0	1680	1240	52	4.47	13.60	1.88	80	596	0.65	0.43
polluted sediments																
JST12							3830	2250	396							
JST13	55.2	/	12.0	/	/	32.8	4030	1770	306	5.45	14.4	2.06	97	653	3.15	0.33

Table 1. *Cont.*

Type	Q	Pl	Ca	D	Py	Cl	Gross-α	Gross-β	^{226}Ra	U	Th	K	^{238}U *	^{40}K *	^{226}Ra/^{238}U *	X *
	%						Bq/kg			μg/g		%	Bq/kg			$A_{K-\beta}/A_{Gross-\beta}$
limestone																
JSY2	1.7	/	85.1	13.2	/	/	375	187	18	2.16	1.20	0.32	38	101	0.47	0.48
JSY3	1.4	/	/	98.6	/	/	599	171	14	1.09	0.84	0.02	19	6	0.72	0.03
JSY4	1.0	/	99.0	/	/	/	316	3640	23	1.66	1.03	1.20	30	380	0.78	0.09
JSY5	1.1	/	11.2	87.7	/	/	106	44	13	0.96	0.51	0.07	17	22	0.76	0.45
JSY6	2.9	/	97.1	/	/	/	244	506	25	2.25	1.54	0.79	40	250	0.62	0.44
JSY7	2.6	/	97.4	/	/	/	318	427	16	2.13	1.47	0.08	38	25	0.42	0.05
JSY8	1.3	/	98.7	/	/	/	702	3680	26	2.94	1.22	1.28	52	406	0.50	0.10
JSY9	0.4	/	18.3	81.3	/	/	265	92	16	1.49	0.62	0.44	27	25	0.60	0.25
JSY10	3.1	/	96.9	/	/	/				2.79	0.91	0.08	50			
JSY11	1.7	/	98.3	/	/	/	418	592	29	2.58	1.72	0.11	46	35	0.63	0.05
shale																
WY	36.9	23.4	/	2.4	4.4	32.9	2280	5380	183	17.20	13.20	3.20	307	1014	0.60	0.17
JSB	45.4	5.5	3.3	3.2	3.2	39.4	2600	1370	114	9.74	12.90	2.99	174	948	0.66	0.62

Notes: ^{40}K*: The radioactivity was calculated based on the content of K and standard radioactivity equations: Abundance of nuclides: ^{39}K (93.2581%), ^{40}K (0.0117%), ^{41}K (6.7302%) [24]; Mass of ^{40}K: $m_{K-40} = \frac{40\times0.0117\%}{39\times93.2581\%+40\times0.0117\%+41\times6.7302\%} \bullet m_K = 0.0001196 m_K$ [25]; Molar mass of ^{40}K: $n = m_{K-40}/M_{K-40}$; Numbers of atoms of ^{40}K: $N = n \cdot N_A$ ($N_A = 6.02 \times 10^{23}$) [26]; (2) Decay rate: $A = -dN/dt = \lambda N$; Decay constant: $\lambda = \ln(2)/t_{1/2}$; $A = N \ln(2)/t_{1/2}$ [26] (half-life of ^{40}K: $t_{1/2} = 1.248 \times 10^9$ y) [24]. ^{238}U *: The radioactivity was calculated as ^{40}K*; abundance of nuclides: ^{238}U (99.2742%), ^{235}U (0.7204%), ^{234}U (0.0054%); half-life of ^{238}U: $t_{1/2} = 4.468 \times 10^9$ y [24]. X *: The fraction of beta emissions from ^{40}K: Decay modes of ^{40}K: β (89.28%) ε (10.72%); $A_{K-\beta} = 0.8928\ A_K$ [24].

Table 2. Gross-α, gross-β and ^{226}Ra activity concentrations (Bq/L) of water samples.

Sample ID	Type of Water	Activity Concentration (Bq/L)		
		Gross-α	Gross-β	^{226}Ra
JSS1	Shallow groundwater	0.06 ± 0.04	0.23 ± 0.02	<0.008
JSS5		0.24 ± 0.05	0.14 ± 0.02	<0.008
JSS8		0.15 ± 0.06	0.09 ± 0.02	<0.008
JSS11		0.12 ± 0.04	0.05 ± 0.01	<0.008
Average		0.14 ± 0.06	0.13 ± 0.07	<0.008
JSS31	Formation water	4.37 ± 0.58	1.4 ± 0.14	0.395 ± 0.011
JSS56	Flowback and produced water	0.29 ± 0.08	0.85 ± 0.11	0.052 ± 0.005
JSS23	Polluted shallow groundwater	0.20 ± 0.08	0.19 ± 0.03	0.038 ± 0.005
China-Guideline	Drinking water	0.5	1	n/a
WHO-Guideline	Drinking water	0.5	1	1

Table 3. Chemical compositions of water samples (TDS = total dissolved solids).

Sample ID	Type of Water	Hydrochemical Type	TDS	Na	Cl	Ba	Sr	Li	U	Th
			(mg/L)	(mg/L)	(mg/L)	(μg/L)	(μg/L)	(μg/L)	(μg/L)	(μg/L)
JSS1	Shallow groundwater	$HCO_3 \cdot SO_4$-Ca	194	21	29	74	152	0.26	0.07	0.10
JSS5		HCO_3-Ca	203	1.6	1.7	15	813	0.29	0.91	0.01
JSS8		HCO_3-Ca·Mg	236	1.4	7.0	22	94	0.82	0.72	0.01
JSS11		HCO_3-Ca·Mg	240	0.9	3.2	13	222	0.89	1.00	0.02
Average			218	6.3	10	31	320	0.56	0.68	0.04
JSS31	Formation water	Cl-Na	62,000	20,800	34,600	907,910	541,964	22,627	<0.002	0.03
JSS56	Flowback and produced water	Cl-Na	581	21.3	270	3691	2416	689	0.08	0.07
JSS23	Polluted shallow groundwater	Cl·HCO_3-Na·Ca	601	150	288	689	1807	450	0.541	0.02
China-Guideline	Drinking water		1000	200	250	700				
WHO-Guideline	Drinking water			200	250	300			30	

4. Results and Discussion

4.1. Radioactivity Characteristics of Soils and Rocks

The statistical activities of gross-α, gross-β, and ^{226}Ra in soil and rock samples are shown in Table 4. The average values of the activity of gross-α in soil, limestone, shale samples were 1547 ± 560, ranging from 591 to 2650 Bq/kg; 371 ± 172, ranging from 106 to 702 Bq/kg; 2440 ranging from 2280 to 2600 Bq/kg, respectively. For gross-β, the activity concentrations in soil, limestone, and shale samples varied from 568 to 2220 Bq/kg, with an average of 1206 ± 408 Bq/kg; 44 to 3680 Bq/kg with an average of 1038 ± 1413 Bq/kg; and 1370 to 5380 Bq/kg, with an average of 3375 Bq/kg, respectively. The average ^{226}Ra values for soil, limestone and shale were 57 ± 19, ranging from 16 to 82 Bq/kg; 20 ± 6, ranging from 13 to 29 Bq/kg; and 149, ranging from 114 to 183 Bq/kg, respectively.

The variability and distribution of gross-α, gross-β, and ^{226}Ra in soil, limestone and shale are shown as boxplots (Figure 2). These plots show the same general activity concentration trend of gross-α, gross-β, ^{226}Ra: shale > soil > limestone, which demonstrates that the radioactivity levels are associated with the soil and rock types.

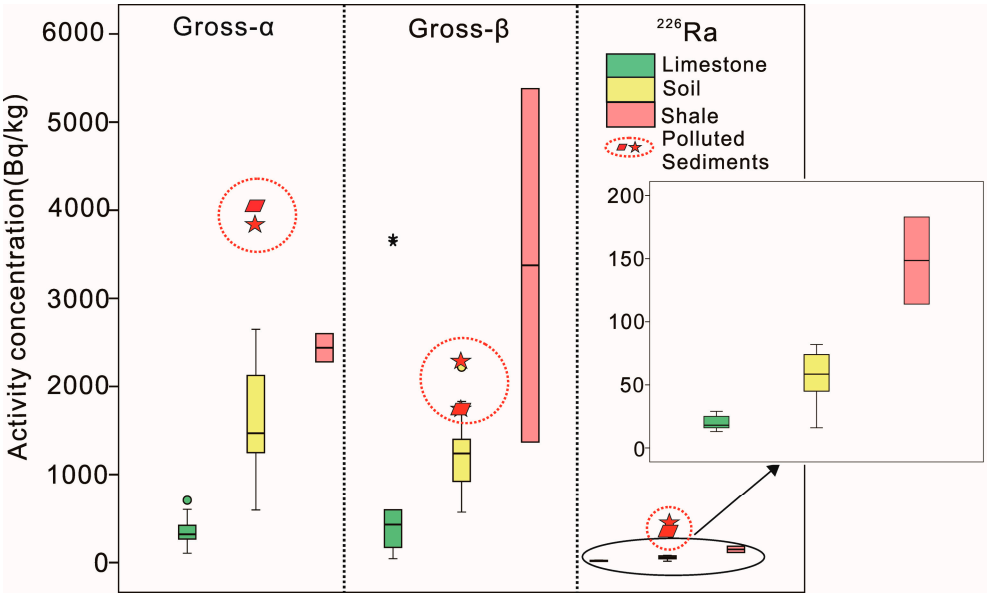

Figure 2. The distribution and variability of gross-α, gross-β, ^{226}Ra in soil, rock and limestone samples ("*" represents extreme values and "○"represents outliers).

By comparison (Table 4), all of the activity concentrations of gross-α and gross-β in the soil in this study compare well with the results of similar studies reported in the Kinta and Segamat Districts, Malaysia [27,28] and Chihuahua City, Mexico [29]. However, compared with Macedonia, the average gross-α and gross-β activity concentrations in this study were nearly three and two times higher, respectively [30]. For ^{226}Ra, the average value in soil is slightly higher than that of other studies except for the Segamat District, Malaysia, but the values of all of the samples overlap the range in China [31,32] and worldwide [33]. For limestone and shale, the published data are limited. The activity concentrations of ^{226}Ra in limestone and shale in the study area are slightly lower than those in Kenya [34]. However, the activity concentrations of ^{226}Ra in the shale in this study are within the results of northern PA in the USA [35]. The difference in radioactivity levels in different areas can be attributed to differences in the local geological and geochemical conditions, especially for soil, and the specific levels are closely related to the type of parent rock [36,37].

Table 4. Average activity concentrations of gross-α, gross-β, ^{226}Ra in soil and rock samples in the study area compared with available databases.

Type	Location	Gross-α (Bq/kg)		Gross-β (Bq/kg)		^{226}Ra (Bq/kg)		Reference
		Range	Average ± SD	Range	Average ± SD	Range	Average ± SD	
Soil	Chongqing, China	591–2650	1547 ± 560	568–2220	1206 ± 408	16–82	57 ± 19	This study
	Kinta District, Malaysia	15–9634	1558	591–4030	1112			[27]
	Segamat District, Malaysia	170–4360	1143 ± 97	70–4690	1071 ± 36	12–968	162 ± 6	[28]
	Macedonia	221–1360	522 ± 192	438–1052	681 ± 146	22–92	39 ± 15	[30]
	Chongqing, China					26–51	35	[32]
	Chihuahua City, Mexico					44–58	52	[29]
	China average					2–426	37 ± 22	[31]
	World average						50	[33]
Polluted sediments	Chongqing, China (JST12, JST13)	3830–4030	3930	1770–2250	2010	306–396	351	This study
Limestone	Chongqing, China	106–702	371 ± 172	44–3680	1038 ± 1413	13–29	20 ± 6	This study
	Chongqing, China						12	[32]
	Kenya					27–45	34 ± 3	[34]
Shale	Chongqing, China	2280–2600	2440	1370–5380	3375	114–183	149	This study
	Kenya						157 ± 17	[34]
	Northern PA, USA					19 ± 2–214 ± 16		[35]

4.2. Association between the Radioactivity Level and Elemental Concentrations

^{238}U, ^{232}Th, ^{40}K and their decay products (e.g., ^{226}Ra, ^{210}Po) are naturally occurring radionuclides that are responsible for the majority of the alpha and beta activity concentrations [12,27]. Therefore, the association between the radioactivity level and elemental concentrations of U, Th, K and other related material is helpful to understand the different radioactivity levels in soils and rocks. Table 5 represents the correlations between the measured parameters in the study area. It was assumed that *R* values between 0.5 and 0.7 indicate a good association [30] and that those between 0.7 and 1.0 indicate a strong association.

Table 5. Matrix of correlation coefficients.

Parameter	Gross-α	Gross-β	^{226}Ra	U	Th	Clay Content
Gross-α	1					
Gross-β	0.37	1				
^{226}Ra	0.73	0.61	1			
U	0.72	0.59	0.96	1		
Th	0.83	0.22	0.69	0.73	1	
Clay content	0.73	0.22	0.69	0.76	0.96	1

The results show a strong correlation between the gross-α and ^{226}Ra activity concentrations (R = 0.73), which demonstrates that ^{226}Ra is an important alpha-emitter. The gross-α activity concentration is closely related to the elemental concentrations of Th (R = 0.83) and U (R = 0.72), which demonstrates that the alpha contributor is a member of both U and Th decay series. However, the correlation between the gross-β and U and Th decay series is not so strong (R from 0.22 to 0.61); this can be explained by the fact that the contribution of U and Th radionuclides to the activity concentration of gross-β is limited. Other beta emitters, such as ^{40}K, which is also widely distributed in nature [27,38], contributes to the activity concentration of gross-β. The average fraction of beta emission from ^{40}K in soil, limestone and shales were 0.55 ± 0.15 , ranging from 0.31 to 0.93; 0.22 ± 0.18, ranging from 0.03 to 0.48; 0.39, ranging from 0.17 to 0.62, respectively by the calculation based on the content of K and standard radioactivity equations [24–26] (Table 1). For ^{226}Ra, the coefficient of correlations (R) between ^{226}Ra and U, ^{226}Ra and Th are 0.96 and 0.69, respectively, which suggests that ^{226}Ra originates from the series decay of ^{238}U in uranium-bearing minerals or organic matter contained in the rocks and soils in situ [12,39]. The values of ^{226}Ra/^{238}U in soil, limestone and shale samples varied from 0.39 to 0.86, with an average of 0.59 ± 0.12; 0.42 to 0.78, with an average of 0.61 ± 0.12; and 0.6 to 0.66, with an average of 0.63, respectively (Table 1). There is a strong positive correlation between the clay content and Th (R = 0.96), U (R = 0.76). For example, the average concentrations of U and Th of shale (13.47, 13.05 μg/g, respectively) is higher than soils (5.79 ± 2.35, 13.56 ± 3.13 μg/g, respectively) and limestone (1.91 ± 0.63, 1.13 ± 0.39 μg/g, respectively) (Table 6), which is corresponding with the trend of clay content: shale (36%) > soil (32%) > limestone (no clay mineral) in this study. It is explained that Th and U are easily absorbed by minerals and organic matter of clay [39]. The concentrations of U and Th increase with elevated clay content. Therefore, the clay content can influence the radioactivity concentration of gross-α, gross-β and ^{226}Ra to different degrees. Compared with limestone (no clay mineral), the shale has a higher clay content (36%), and a higher radioactivity level.

Table 6. Elemental concentration of U, Th and K in soil and rock samples.

Type	Number of Sample	U (μg/g)		Th (μg/g)		K (%)	
		Range	Average ± SD	Range	Average ± SD	Range	Average
Soil	16	1.59–9.55	5.79 ± 2.35	6.37–17.70	13.56 ± 3.13	0.24–3.09	1.40 ± 0.46
Limestone	9	0.96–2.94	1.91 ± 0.63	0.51–1.72	1.13 ± 0.39	0.02–1.28	0.56 ± 0.48
Shale	2	9.74–17.20	13.47	12.90–13.20	13.05	0.01–7.06	2.03

In the study area, the concentrations of U, Th and K have the same trend: shale > soil > limestone (Table 6). This is due to the absorption, complexation and ion exchange of clay minerals and organic matter in shale; therefore, it is reasonable that the same general activity concentration trend of gross-α, gross-β, and ^{226}Ra: shale > soil > limestone, which was concluded above.

4.3. Radioactivity of Water

The activity concentrations of gross-α, gross-β and ^{226}Ra in water samples from the limestone aquifer (shallow groundwater), shale formation targeted for shale gas productions (formation water), and flowback fluid in the study area are shown in Table 2. The activity concentrations of gross-α in shallow groundwater vary from 0.06 ± 0.04 to 0.24 ± 0.05 Bq/L, with an average value of 0.14 ± 0.06 Bq/L. For gross-β, the activity concentrations in shallow groundwater range from 0.05 ± 0.01 to 0.23 ± 0.02 Bq/L, with an average value of 0.13 ± 0.07 Bq/L. The activity concentrations of ^{226}Ra are all less than 0.008 Bq/L. These results show that the activity concentrations of gross-α, gross-β and ^{226}Ra in the shallow groundwater are all below the drinking water standards of China (GB5749-2006) and/or the WHO guideline values.

As for formation water with the total dissolved solids (TDS) of 62 g/L, the activity concentrations of gross-α and gross-β are nearly 9 times and 1.5 times higher than the drinking water standards of China. However, the activity concentration of ^{226}Ra of 0.395 Bq/L is far lower than the WHO guideline value (1 Bq/L; there is not a standard line for drinking water in China), but higher than the average value of shallow groundwater from the limestone aquifer (less than 0.008 Bq/L). It is noted that the reported radioactivities of ^{226}Ra in the Formation water (JSS31) and Early flowback fluid (JSS23) measured by $BaSO_4$ coprecipitation method may be lower than the real values due to the interference of high concentrations of Ba [10].

The activity concentrations of gross-α, gross-β and ^{226}Ra in the flowback and produced fluid are all below the drinking water standards of China and the WHO guideline values, but higher than the average values of shallow groundwater (Table 2). The higher radioactivity levels may be associated with the formation targeted for shale gas production [9,13] or dilution of the formation water by freshwater from hydraulic fracturing (Figure 3) [13]. The specific signatures of TDS, Na, Cl, Sr, Ba and Li also imply a mixing process between the formation water and freshwater (Figure 4).

The activity concentrations of gross-α, gross-β and ^{226}Ra in the formation water are much higher than those of other types of water. However, the concentrations of U and Th are far lower (Tables 2 and 3). U and Th are essentially immobile with low concentrations in the reducing conditions of formation waters [40–42]. Therefore, the high activity concentrations of gross-α, gross-β and ^{226}Ra in formation water originate directly from the radioactive decay of the radionuclides in the host formation with high U and Th. For ^{226}Ra, it is the decay product of ^{238}U in uranium-bearing minerals or organic matter contained in the host formation [13], alpha-recoil damage to the host phase allows Ra to enter pore water [43]. Thus, the high concentrations of U and Th in the shale formation lead to more ^{226}Ra in the formation water. Besides, the chemical compositions of the formation water and flowback fluids can improve the aqueous phase concentrations of Ra^{2+}, since the high concentrations of divalent cations, particularly Ba^{2+}, compete with Ra^{2+} for adsorption on solid minerals' surface [44]. Figure 3 shows a positive correlation between the activity concentrations and Cl concentration or TDS (not shown), which are consistent with other studies [13].

The activity concentrations of gross-α, gross-β, ^{226}Ra in the formation water in the study area are far lower than results of other areas in the USA (with ranges from 86 to 678, 23 to 77, and 16 to 500 Bq/L, respectively, Table 7) [13,45]. It because that the uranium content in the Marcellus shale in the USA is higher comparing with the shale of the study area due to its geologic origins (sources and mechanisms of enrichment of uranium, such as the content of organic matter, the action of hydrogen sulfide, phosphate and other chemical variables) [46], which causing higher the radioactivity of formation water in the USA. There are also large differences in the formation water from different reservoirs of the Marcellus Shale at different areas (Table 7). These differences are likely due to amounts of U- and

Th-enriched materials within reservoirs, rather than bulk strata, which are the major source of high NORM activities in formation water. Mixing with lower NORM fracturing fluids may be another factor [47]. Compared with the USA, the lower radioactivity level of the formation water in the study area will lead to less contamination of soil and shallow groundwater if a contamination happens in the same possible way [1,48].

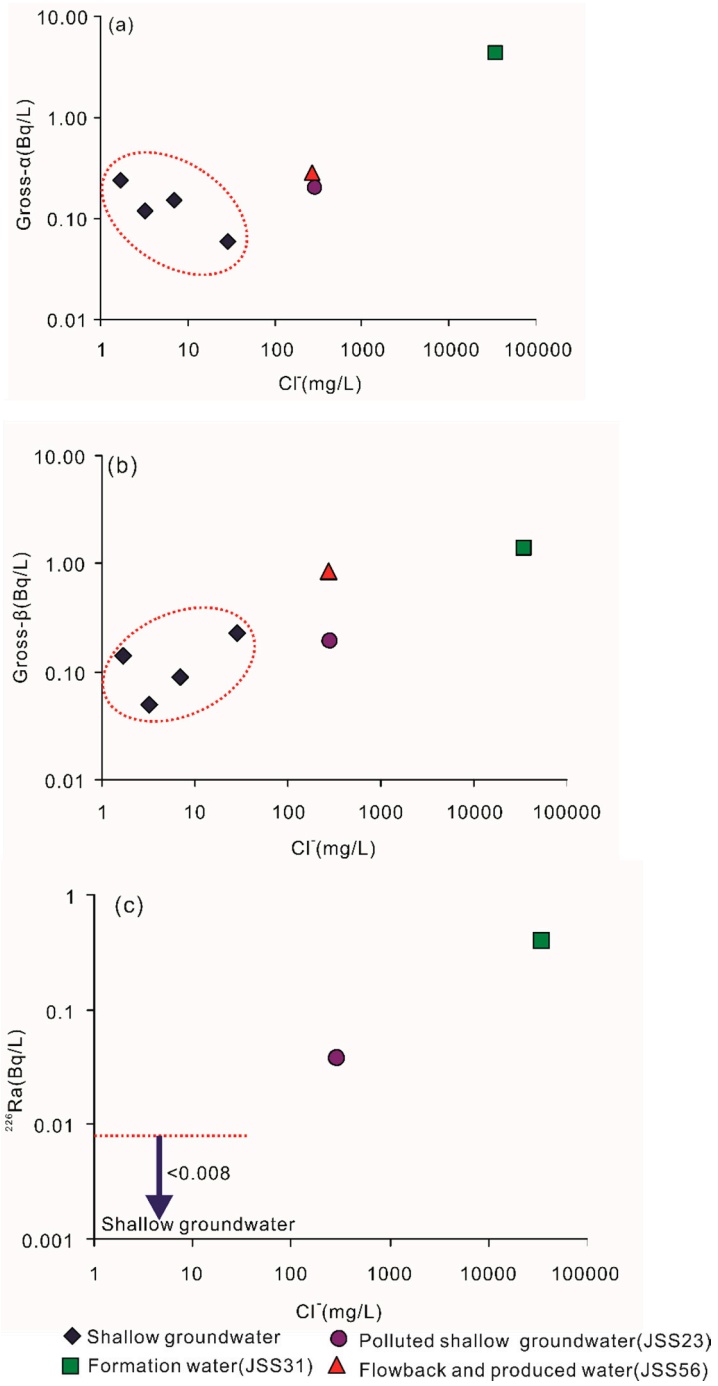

Figure 3. The activity concentration of: gross-α (**a**); gross-β (**b**); and ^{226}Ra (**c**) versus Cl concentration for shallow groundwater, flowback and produced water (JSS56), polluted shallow groundwater (JSS23) and formation water (JSS31).

Table 7. Gross-α, gross-β, ^{226}Ra activities and TDS concentration in samples of formation water in the study area and USA.

Location	Producing Formation	Formation Age	Gross-α (Bq/L)	Gross-β (Bq/L)	^{226}Ra (Bq/L)	TDS (g/L)	Method and Reference
Chongqing, China	Longmaxi Shale	Lower Silurian	4.37	1.40	0.395	62	Coprecipitation with $BaSO_4$ (This study)
Lycoming, USA	Marcellus Shale	Middle Devonian	228 ± 27	49 ± 7	16 ± 0.4	62	EPA900.0Mod., 903.1,904.0 [13]
Washington, USA	Marcellus Shale	Middle Devonian			47 ± 5	200	EPA901.1Mod. [13]
Westmoreland, USA	Marcellus Shale	Middle Devonian	86 ± 30	77 ± 34	38 ± 7	116	EPA900.0,903.0,904.0 [13]
Schuyler, USA	Marcellus Shale	Middle Devonian	678 ± 137		500 ± 98	205	[45]
Steuben, USA	Marcellus Shale	Middle Devonian	147 ± 41	23 ± 22	192 ± 58		[45]
Greene, USA	Marcellus Shale	Middle Devonian			195 ± 3		Coprecipitation with $BaSO_4$; γ-spectrometry [13]

4.4. The Potential Contamination of Soil and Shallow Groundwater

It is noted that the activity concentrations of gross-α and gross-β (0.20 ± 0.08 and 0.19 ± 0.03 Bq/L, respectively) in the polluted groundwater sample (JSS23) (Table 3) are slightly higher than the average value of other shallow groundwater samples (0.14 ± 0.06, 0.13 ± 0.07 Bq/L). For ^{226}Ra, the activity concentration (0.038 ± 0.005 Bq/L) is higher than that of groundwater (less than 0.008 Bq/L). The elevated radioactivity of JSS23 resulted from drilling fluid leakage, which is further confirmed by its geochemical characteristics. The geochemical type of the shallow groundwater sample JSS23 ($Cl{\cdot}HCO_3$-Na·Ca) is different from other shallow groundwaters (Table 3). In addition, the highly specific signatures of TDS, Na, Cl, Sr, Ba and Li imply that the shallow groundwater JSS23 has mixed with saline water, causing salinization of JSS23 groundwater (Figure 4). Compared with gross-α and gross-β, ^{226}Ra can better represent the contamination degree of shallow groundwater by formation water or flowback fluid (Figure 3).

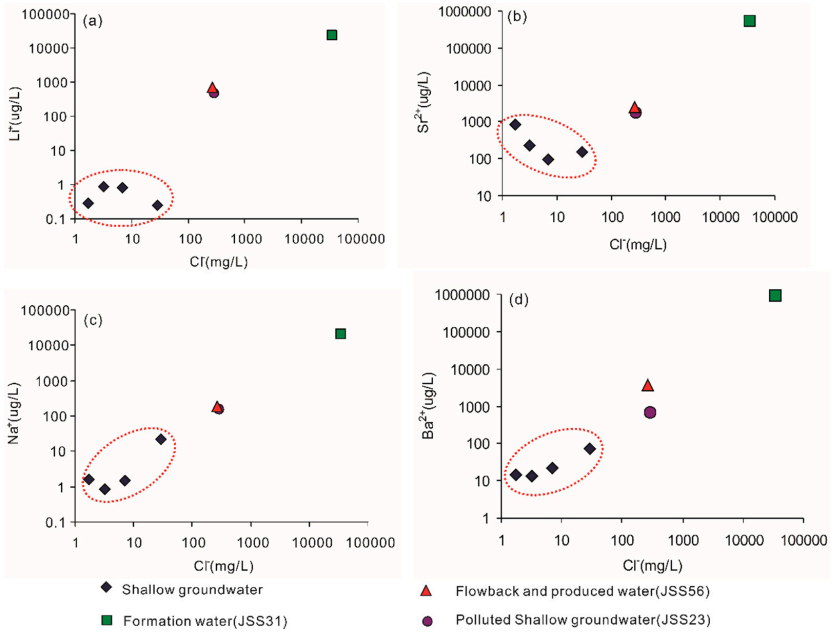

Figure 4. Li (**a**); Sr (**b**); Na (**c**); and Ba (**d**) versus Cl concentration for shallow groundwater, flowback and produced water (JSS56), polluted shallow groundwater (JSS23) and formation water (JSS31).

Due to the pollution of groundwater JSS23, the average gross-α, gross-β, and ^{226}Ra activity concentrations of polluted stream sediments (JST12 and JST13) are 2.5, 1.7 and 6.2 times higher than the average values of background soil, respectively. The calculated value of ^{226}Ra/^{238}U for sample JST13 is 3.15, much higher than the average value (0.59 ± 0.12) in soil (Table 1). Although the pollution degree in the study area is not significant, the contamination cannot be neglected. When saline waters (drilling fluids, flowback and produced water, or formation water) mix with shallow groundwater and surface water by spills and leaks or other possible ways [1,48], the Ra can be absorbed and retained in sediments, because Ra adsorption increases with decreasing salinity, especially heavier alkaline earth metals (Ba and Sr) [10,44]. For example, the radioactivity level of ^{226}Ra in stream sediments at the point of discharge of a waste treatment facility in the central Pennsylvania of the USA is nearly 200 times greater than those of upstream and background sediments [9]. The case is not common at other study areas; however, it implies that there is a potential risk of soil and shallow groundwater contamination during shale gas exploitation. Therefore, the baseline data of soil and groundwater are necessary for environmental assessments in the future, which can reduce the debate on the environmental impacts of shale gas exploitation [48,49].

5. Conclusions

Naturally occurring radioactive materials (NORM) are notable concerns of the complex contaminants in groundwater and soil caused by shale gas exploitation; however, there is a lack of baseline radioactivity level research prior to shale gas exploitation in the Fuling block, Chongqing, SW China. This study assessed the radioactivity levels of soils, rocks, and waters and established the relationship of radioactivity between waters and their reservoirs.

For soils and rocks, the radiation levels showed the same general activity concentration trend of gross-α, gross-β, and ^{226}Ra: shale > limestone > soil, corresponding to the trend of uranium, thorium and potassium concentrations, which demonstrated that the radioactivity level is associated with the soil and rock types. In addition, the concentrations of uranium and thorium increase with increasing clay content. Therefore, the clay content influences the radioactivity concentrations of gross-α, gross-β and ^{226}Ra to different degrees.

The average activity concentrations of gross-α, gross-β and ^{226}Ra of shallow groundwater from a limestone aquifer (0.14 ± 0.06, 0.13 ± 0.07, <0.008 Bq/L, respectively) are all below the drinking water standards of China and WHO guideline values. These results can be viewed as the baseline characteristics of shallow groundwater radioactivity concentrations in the study area. The radioactivity concentrations of gross-α, gross-β, and ^{226}Ra of the formation saline (4.37 ± 0.58, 1.40 ± 0.14, and 0.375 ± 0.011 Bq/L, respectively) are higher than that of shallow groundwater. Compared with other studies carried out in the Marcellus Shale, USA (whose gross-α, gross-β and ^{226}Ra values range from 86 ± 30 to 678 ± 137, 0 to 77 ± 34, and 16 ± 0.4 to 500 ± 98 Bq/L, respectively), the activity concentrations in the study area are far lower. Thus, the lower radioactivity levels of formation water in the study area lead to less contamination of soil and shallow groundwater than in the USA if a contamination happens in the same possible way. In addition, there is a positive correlation between the radioactivity concentrations and Cl (or TDS) concentration.

Pollution in both the soil and groundwater in the study area suggest that there is a potential risk of contamination of soil and shallow groundwater during shale gas exploitation. Compared with gross-α and gross-β, the activity concentration of ^{226}Ra can be more effectively used to identify the possible contamination.

Acknowledgments: This work was supported by the "Strategic Priority Research Program (B)" of the Chinese Academy of Sciences (Grant XDB10030603) and the National Natural Science Foundation of China (Grants 41672254 and 41202183). The authors wish to express Xiao Li, Fengshan Ma, Liman Li, Jiao Tian and Yingchun Wang for their help during fieldwork.

Author Contributions: Tianming Huang conceived and designed the experiments; Tianming Huang and Shuo Yang performed the experiments; Yinlei Hao and Zhonghe Pang analyzed the data; Zhenbin Li contributed analysis tools; and Tianming Huang and Yinlei Hao wrote the paper.

Conflicts of Interest: The authors declare no conflict of interest.

References

1. Vengosh, A.; Jackson, R.B.; Warner, N.; Darrah, T.H.; Kondash, A. A critical review of the risks to water resources from unconventional shale gas development and hydraulic fracturing in the United States. *Environ. Sci. Technol.* **2014**, *48*, 8334–8348. [CrossRef] [PubMed]
2. Finkel, M.L.; Law, A. The rush to drill for natural gas: A public health cautionary tale. *Am. J. Public Health* **2011**, *101*, 784–785. [CrossRef] [PubMed]
3. Goldstein, B.D.; Kriesky, J.; Pavliakova, B. Missing from the table: Role of the environmental public health community in governmental advisory commissions related to Marcellus Shale drilling. *Environ. Health Perspect.* **2012**, *120*, 483–486. [CrossRef] [PubMed]
4. Warner, N.R.; Jackson, R.B.; Darrah, T.H.; Osborn, S.G.; Down, A.; Zhao, K.; White, A.; Vengosh, A. Geochemical evidence for possible natural migration of Marcellus Formation brine to shallow aquifers in Pennsylvania. *Proc. Nat. Acad. Sci. USA* **2012**, *109*, 11961–11966. [CrossRef] [PubMed]
5. Zhang, D.; Yang, T. Environmental impacts of hydraulic fracturing in shale gas development in the United States. *Pet. Explor. Dev.* **2015**, *42*, 876–883. [CrossRef]
6. Nelson, A.W.; Eitrheim, E.S.; Knight, A.W.; May, D.; Mehrhoff, M.A.; Shannon, R.; Litman, R.; Burnett, W.C.; Forbes, T.Z.; Schultz, M.K. Understanding the Radioactive Ingrowth and Decay of Naturally Occurring Radioactive Materials in the Environment: An Analysis of Produced Fluids from the Marcellus Shale. *Environ. Health Perspect.* **2015**, *123*, 689–696. [CrossRef] [PubMed]
7. Brown, V.J. Radionuclides in fracking wastewater: Managing a toxic blend. *Environ. Health Perspect.* **2014**, *122*, A50–A55. [CrossRef] [PubMed]
8. Levinthal, J.D.; Richards, B.; Snow, M.S.; Watrous, M.G.; McDonald, L.W., IV. Correlating NORM with the mineralogical composition of shale at the microstructural and bulk scale. *Appl. Geochem.* **2017**, *76*, 210–217. [CrossRef]
9. Warner, N.R.; Kresse, T.M.; Hays, P.D.; Down, A.; Karr, J.D.; Jackson, R.B.; Vengosh, A. Geochemical and isotopic variations in shallow groundwater in areas of the Fayetteville Shale development, north-Central Arkansas. *Appl. Geochem.* **2013**, *35*, 207–220. [CrossRef]
10. Nelson, A.W.; May, D.; Knight, A.W.; Eitrheim, E.S.; Mehrhoff, M.; Shannon, R.; Litman, R.; Schultz, M.K. Matrix Complications in the Determination of Radium Levels in Hydraulic Fracturing Flowback Water from Marcellus Shale. *Environ. Sci. Technol.* **2014**, *1*, 204–208. [CrossRef]
11. Haluszczak, L.O.; Rose, A.W.; Kump, L.R. Geochemical evaluation of flowback brine from Marcellus gas wells in Pennsylvania, USA. *Appl. Geochem.* **2013**, *28*, 55–61. [CrossRef]
12. Nelson, A.W.; Knight, A.W.; Eitrheim, E.S.; Schultz, M.K. Monitoring radionuclides in subsurface drinking water sources near unconventional drilling operations: A pilot study. *J. Environ. Raioact.* **2015**, *142*, 24–28. [CrossRef] [PubMed]
13. Rowan, E.L.; Engle, M.A.; Kirby, C.S.; Kraemer, T.F. *Radium Content of Oil- and Gas-Field Produced Waters in the Northern Appalachian Basin (USA)—Summary and Discussion of Data*; Scientific Investigations Report; U.S. Geological Survey: Reston, VA, USA, 2011; Volume 31, pp. 2011–5135.
14. China Geological Survey, 2015. The Shale Gas Resources in China. Geological Survey Report. Available online: http://www.ngac.cn/GTInfoShow.aspx?InfoID=5126&ModuleID=73&PageID=1 (accessed on 28 June 2015).
15. MLRC—The Ministry of Land and Resources of China. Shale Gas Planning (2016–2020). Available online: http://www.mlr.gov.cn/xwdt/kyxw/201610/t20161013_1419140.htm (accessed on 13 October 2016).
16. Li, Y.; Huang, T.; Pang, Z.; Wang, Y.; Jin, C. Geochemical Characteristics of Shallow Groundwater in Jiaoshiba Shale Gas Production Area: Implications for Environmental Concerns. *Water* **2016**, *8*, 552. [CrossRef]
17. Guo, X.S. *Shale Gas Enrichment Mechanism and Exploration Technology in Jiaoshi Block of Fuling Gas Field*; Science Press: Beijing, China, 2009. (In Chinese)

18. Lv, Y.X.; Hu, W.; Zhou, J. Analysis on karst development law and its influencing factors in Jiaoshi area of Chongqing city. *China J. Geol. Hazard Control* **2012**, *23*, 59–63. (In Chinese).
19. Zhuo, W.; Iida, I.; Yang, X. Occurrence of ^{222}Rn, ^{226}Ra, ^{228}Ra and U in groundwater in Fujian Province, China. *J. Environ. Radioact.* **2001**, *53*, 111–120. [CrossRef]
20. Dong, Q.; Dong, C.; Guo, D.; Fan, Z.; Tian, F.; Hu, X.; Pan, J.; Wang, T. Determing Experiment of Radium in Standard Samples with Updated Radium-Randon Analyzer PC-2100. *Uranium Geol.* **2014**, *30*, 51–56.
21. Currie, L.A. Limits for Qualitative Detection and Quantitative Determination. *Appl. Chem.* **1968**, *40*, 586–593.
22. Maxwell, S.L., III. Rapid method for 226Ra and 228Ra analysis in water samples. *J. Radioanal. Nucl. Chem.* **2006**, *270*, 651–655. [CrossRef]
23. Maxwell, S.L., III; Culligan, B.K.; Warren, R.A.; McAlister, D.R. Rapid method for the determination of ^{226}Ra in hydraulic fracturing wastewater samples. *J. Radioanal. Nucl. Chem.* **2016**, *309*, 1333–1340. [CrossRef]
24. NNDC: Chart of Nuclides. Available online: http://www.nndc.bnl.gov/chart/ (accessed on 2 April 2017).
25. Fan, S.; Dai, L. New statistics of Natural elements and nuclides. *J. Changchun Univ. Earth Sci.* **1982**, *1*, 53–66. (In Chinese).
26. Choppin, G.; Liljenzin, J.O.; Rydberg, J. *Radiochemistry and Nuclear Chemistry*, 3rd ed.; Butterworth-Heinemann: Oxford, UK, 2002; pp. 79–83.
27. Lee, S.K.; Wagiran, H.; Ramli, A.T. A survey of gross alpha and gross beta activity in soil samples in Kinta District, Perak, Malaysia. *Radiat. Prot. Dosim.* **2014**, *162*, 345–350. [CrossRef] [PubMed]
28. Saleh, M.A.; Ramli, A.T.; Alajerami, Y.; Aliyu, A.S. Assessment of environmental ^{226}Ra, ^{232}Th and ^{40}K concentrations in the region of elevated radiation background in Segamat District, Johor, Malaysia. *J. Environ. Radioact.* **2013**, *124*, 130–140. [CrossRef] [PubMed]
29. Sergio, L.G.; Angelica, P.T.; Carmelo, P.A.; Jorge, C.F.; Maria Elena, M.C.; Marusia, R.V. Lifetime Effective Dose Assessment Based on Background Outdoor Gamma Exposure in Chihuahua City, Mexico. *Int. J. Environ. Res. Public Health* **2015**, *12*, 12324–12339.
30. Dimovska, S.; Stafilov, T.; Sajn, R. Radioactivity in soil from the city of Kavadarci (Republic of Macedonia) and its environs. *Radiat. Prot. Dosim.* **2011**, *148*, 107–120. [CrossRef] [PubMed]
31. The Writing Group for the Summary Report on Nationwide Survey of Environmental Radioactivity Level in China. Investigation of natural radionuclide contents in soil in China (1983–1990). *Radiat. Prot.* **1992**, *12*, 122–141, (In Chinese with English Abstract).
32. Zheng, Y. Study on Environment Radioactivity of Representative Diggings in ChongQing. Master's Thesis, Chongqing University, Chongqing, China, 2007.
33. United Nations Scientific Committee on the Effects of Atomic Radiation. *Sources, Effects and Risks of Ionizing Radiation*; Report to the General Assembly with Annex B; United Nations: New York, NY, USA, 1988.
34. Mustapha, A.O.; Patel, J.P.; Rathore, I.V.S. Assessment of Human Exposures to Natural Sources of Radiation in Kenya. *Radiat. Prot. Dosim.* **1999**, *82*, 285–292. [CrossRef]
35. Eitrheim, E.S.; May, D.; Forbes, T.Z.; Nelson, A.W. Disequilibrium of Naturally Occurring Radioactive Materials (NORM) in Drill Cuttings from a Horizontal Drilling Operation. *Environ. Sci. Technol. Lett.* **2016**, *3*, 425–429. [CrossRef]
36. Xinwei, L.; Lingqing, W.L.; Xiaodan, J.; Leipeng, Y.; Gelian, D. Specific activity and hazards of Archeozoic-Cambrian rock samples collected from the Weibei area of Shaanxi, China. *Radiat. Prot. Dosim.* **2006**, *118*, 352–359. [CrossRef] [PubMed]
37. Faanu, A.; Lawluvi, H.; Kpeglo, D.O.; Darko, E.O.; Emi-Reynolds, G.; Awudu, A.R.; Adukpo, O.K.; Kansaana, C.; Ali, I.D.; Agyeman, B.; et al. Assessment of natural and anthropogenic radioactivity levels in soils, rocks and water in the vicinity of Chirano gold mine in Ghana. *Radiat. Prot. Dosim.* **2014**, *158*, 87–99. [CrossRef] [PubMed]
38. Lee, S.K.; Wagiran, H.; Ramli, A.T.; Apriantoro, N.H.; Wood, A.K. Radiological monitoring: Terrestrial natural radionuclides in Kinta District, Perak, Malaysia. *J. Environ. Raioact.* **2009**, *100*, 368–374. [CrossRef] [PubMed]
39. Liu, Y.; Cao, L.; Li, Z.; Wang, H.; Chu, T.; Zhang, J. *Element Geochemistry*; Science Press: Beijing, China, 1984; pp. 216–238. (In Chinese)
40. Atkins, M.L.; Santos, I.R.; Perkins, A.; Maher, D.T. Dissolved radon and uranium in groundwater in a potential coal seam gas development region(Richmond River Catchment Australia). *J. Environ. Raioact.* **2016**, *154*, 83–92. [CrossRef] [PubMed]

41. Rogers, J.J.W.; Adams, J.A.S. Thorium. In *Handbook of Geochemistry*; Wedepohl, K.H., Ed.; v. II/5 (Chapter 90-D, Table 90-D-1); Springer: New York, NY, USA, 1969.
42. Rogers, J.J.W.; Adams, J.A.S. Uranium. In *Handbook of Geochemistry*; Wedepohl, K.H., Ed.; v. II/5 (Chapter 92-D, Table 92-D-1); Springer: New York, NY, USA, 1969.
43. Rama; Moore, W.S. Mechanism of transport of U-Th series radioisotopes from solids into ground water. *Geochim. Cosmochim. Acta* **1984**, *48*, 395–399.
44. Nelson, A.W.; Johns, A.W.; Eitrheim, E.S.; Knight, A.W.; Basile, M.; Arthur Bettis, E., III; Schultz, M.K.; Forbes, T.Z. Partitioning of naturally-Occurring radionuclides(NORM) in Marcellus Shale produced fluids influenced by chemical matrix. *Environ. Sci. Process. Impacts* **2016**, *18*, 456. [CrossRef] [PubMed]
45. NYSDEC-New York State Department of Environmental Conservation (2009). Draft Supplemental Generic Environmental Impact Statement (SGEIS) on the Oil, Gas, And Solution Mining Regulatory Program (September 2009), Well Permit Issuance for Horizontal Drilling and High-Volume Hydraulic Fracturing to Develop the Marcellus Shale and Other Low-Permeability Gas Reservoirs: New York State Department of Environmental Conservation, Division of Mineral Resources, Bureau of Oil and Gas Regulation, Appendix 13, NYS Marcellus Radiological Data from Production Brine, 2011. Available online: http://www.dec.ny.gov/energy/58440.html (accessed on 12 November 2016).
46. Swanson, V.E. *Geology and Geochemistry of Uranium in Marine Black Shales, a Review*; U.S. Geological Survey Professional Paper 356-C; United States Government Printing Office: Washington, DC, USA, 1961.
47. Barbot, E.N.; Vidic, N.S.; Gregory, K.B.; Vidic, R.D. Spatial and Temporal Correlation of Water Quality Parameters of Produced Waters from Devonian-Age Shale Following Hydraulic Fracturing. *Environ. Sci. Technol.* **2013**, *47*, 2562–2569. [CrossRef] [PubMed]
48. Vidic, R.D.; Brantley, S.L.; Vandenbossche, J.M.; Yoxtheimer, D.; Abad, J.D. Impact of shale gas development on regional water quality. *Science* **2013**, *340*, 1235009. [CrossRef] [PubMed]
49. Osborn, S.G.; Vengosh, A.; Warner, N.R.; Jackson, R.B. Methane contamination of drinking water accompanying gas-Well drilling and hydraulic fracturing. *Proc. Nat. Acad. Sci. USA* **2011**, *108*, 8172–8176. [CrossRef] [PubMed]